Available online at www.sciencedirect.com
ScienceDirect
Nuclear Medicine and Biology 37 (2010) 517–526
NUCLEAR MEDICINE — AND — BIOLOGY
www.elsevier.com/locate/nucmedbio

Preclinical evaluation of an ^{18}F-labelled β_1-adrenoceptor selective radioligand based on ICI 89,406

Marilyn P. Law[a,c,*], Stefan Wagner[a], Klaus Kopka[a], Christiane Renner[a], Victor W. Pike[b], Otmar Schober[a], Michael Schäfers[c]

[a]*Department of Nuclear Medicine, University Hospital Münster, D-48149 Münster, Germany*
[b]*Molecular Imaging Branch, National Institute of Mental Health, National Institutes of Health, Bethesda, MD 20892-1003, USA*
[c]*European Institute of Molecular Imaging, D-48149 Münster, Germany*

Received 18 November 2009; received in revised form 21 December 2009; accepted 18 January 2010

Abstract

Purpose: Radioligand binding studies indicate a down-regulation of myocardial β_1-adrenoceptors (β_1-AR) in cardiac disease which may or may not be associated with a decrease in β_2-ARs. We have chosen ICI 89,406, a β_1-selective AR antagonist, as the lead structure to develop new β_1-AR radioligands for PET and have synthesised a fluoro-ethoxy derivative (F-ICI).
Methods: (*S*)-*N*-[2-[3-(2-Cyano-phenoxy)-2-hydroxy-propylamino]-ethyl]-*N*′-[4-(2-[^{18}F]fluoro-ethoxy)-phenyl]-urea ((*S*)-[^{18}F]F-ICI) was synthesised. Myocardial uptake of radioactivity after intravenous injection of (*S*)-[^{18}F]F-ICI into adult CD_1 mice or Wistar rats was assessed with positron emission tomography (PET) and postmortem dissection. Metabolism was assessed by high-performance liquid chromatography analysis of plasma and urine.
Results: The heart was visualised with PET after injection of (*S*)-[^{18}F]F-ICI but neither unlabelled F-ICI nor propranolol (non-selective β-AR antagonist) injected 15 min after (*S*)-[^{18}F]F-ICI affected myocardial radioactivity. Ex vivo dissection demonstrated that predosing with propranolol or CGP 20712 (β_1-selective AR-antagonist) did not affect myocardial radioactivity. Radiometabolites rapidly appeared in plasma and both (*S*)-[^{18}F]F-ICI and radiometabolites accumulated in urine.
Conclusions: Myocardial uptake of (*S*)-[^{18}F]F-ICI after intravenous injection was mainly at sites unrelated to β_1-ARs. (*S*)-[^{18}F]F-ICI is not a suitable β_1-selective-AR radioligand for PET.

Keywords: [^{18}F]Fluoroethoxy-ICI 89,406 for PET; β_1-adrenoceptor-selective radioligand; PET radioligand; Myocardial β_1-adrenoceptors; Small animal PET

1. Introduction

It is generally accepted that the sympathetic nervous system plays a role in the development of heart failure. Overactivation of the cardiac sympathetic nerves causes an increased release of noradrenaline from the heart to plasma [1–3]. Myocardial β-adrenoceptor (β-AR) density is reduced and downstream mechanisms altered. Clinical trials have shown that β-AR antagonists, such as metropolol, carvedilol and bisoprolol, reduce morbidity and mortality of human heart failure [1,3].

Many studies of myocardial membranes obtained at autopsy or surgery have demonstrated a preferential down regulation of β_1-AR [4–7]. Decreases in both β_1- and β_2-ARs, however, have been reported [5–8], and it is not clear whether or not there is a clinical advantage of β_1-AR antagonist therapy [1,3]. In addition genetic polymorphisms of β_1- and β_2-AR may be risk factors which influence the progression of heart failure [9]. A better understanding of the roles of each sub-type may help to improve therapy.

Positron emission tomography (PET) with the non-selective β-AR radioligand (*S*)-[^{11}C]CGP 12177 has been used to demonstrate down-regulation of myocardial β-ARs in vivo in patients with some types of heart disease, including hypertrophic cardiomyopathy, idiopathic right ventricular outflow tract tachycardia and arrhythmogenic

* Corresponding author. Tel.: +49 251 8347362; fax: +49 251 8347363.
E-mail address: mplaw@uni-muenster.de (M.P. Law).

0969-8051/$ – see front matter © 2010 Elsevier Inc. All rights reserved.
doi:10.1016/j.nucmedbio.2010.01.004

right ventricular cardiomyopathy [10–12] but not Brugada syndrome [13], and a newer more easily prepared radioligand [^{11}C]CGP 12388 is now available [14,15]. Although several groups have been searching for a β_1-selective-AR radioligand for PET, none has succeeded [16].

We have chosen ICI 89,406 (Fig. 1A), a β_1-AR-selective antagonist [17–19], as our lead compound for developing β_1-AR-selective ligands for molecular imaging. Twenty derivatives were prepared by modifying the aromatic substituents and lengths of the aliphatic chains. Of these, 16 derivatives were selective for β_1-ARs (high affinity inhibition constant for β_1-ARs K_{i1}, 0.02–35 nM; low affinity inhibition constant for β_2-ARs K_{i2}, 12–16,000 nM; β_1-selectivity K_{i1}/K_{i2}, 35–16,800) [20]. One derivative, I-ICI-H [21], iodinated at ring A (Fig. 1A) by exchanging the cyano moiety for iodine, showed especially high affinity and selectivity in vitro but the radioactive compound [$^{123/125}$I]I-ICI-H was not suitable for in vivo studies due to high nonspecific binding [21]. A more hydrophilic iodinated derivative, I-ICI-COOH, was synthesised, but although this compound again showed high affinity and selectivity in vitro, it was rapidly de-iodinated in vivo [22]. A third derivative, (*S*)-[^{11}C]ICI-OMe, with a [^{11}C] methoxy moiety at C4 of ring B (Fig. 1A) was taken up by the heart in mice and rats but uptake was not displaced or blocked by established β-AR antagonists, indicating that uptake was not specific to β-ARs. In addition, there was metabolism to [^{11}C]CO_2 [23].

Other radiolabelled analogues of ICI 89,406 may be less susceptible to metabolism. An ^{18}F-labelled compound would have the advantage of a longer radioactive half life than ^{11}C so that biochemical pathways could be followed for longer times. In addition, the spacial resolution for ^{18}F-labelled ligands is superior due to the shorter positron range for ^{18}F compared to ^{11}C. Substitution of the CN moiety in ring A (Fig. 1) by fluorine is theoretically feasible. However, by analogy with I-ICI-H, the resulting compound may show high non-specific binding. Introduction of [^{18}F]fluorine in ring B (Fig. 1B) was an alternative option. Although the [^{11}C]-OMe derivative was metabolised to $^{11}CO_2$, presumably via [^{11}C]methanol and the Krebs cycle [22], the fluorinated derivative may be metabolised less rapidly by an alternative pathway enabling sufficient radiolabelled ligand to be available for β_1-AR binding. We have, therefore, synthesised the fluorinated analogues (*R*)- and (*S*)-*N*-[2-[3-(2-cyano-phenoxy)-2-hydroxy-propylamino]-ethyl]-*N*′-[4-(2-fluoro-ethoxy)-phenyl]-urea (Fig. 1B) [24]. In vitro studies showed that the (*S*)-enantiomer had higher β_1-AR selectivity and affinity than the (*R*)-enantiomer (affinity K_{i1}=0.049 nM vs K_{i1}=0.297 nM; selectivity 40,800 vs. 1580) [24]. The affinity and selectivity of the (*S*)-enantiomer were also higher than those for (*S*)-ICI-OMe (K_{i1}=0.07, selectivity=1240, respectively) [25]. The ^{18}F-labelled (*S*)-analogue [(*S*)-[^{18}F]F-ICI] was synthesised at a higher specific activity [40 GBq·μmol^{-1} at end of synthesis (EOS)] [24] than was achieved for (*S*)-ICI-OMe (6.5 GBq·μmol^{-1} at EOS) [25].

The present article describes experiments to evaluate the suitability of (*S*)-[^{18}F]F-ICI for PET in mice and rats using small animal PET, ex vivo dissection and high-performance liquid chromatography (HPLC) analysis of radioactive metabolites.

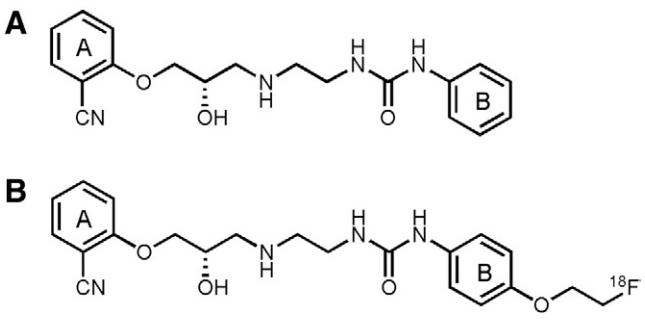

Fig. 1. Structure of the β_1-adrenoceptor antagonist ICI 89,406 (A) and its derivative (*S*)-*N*-[2-[3-(2-cyano-phenoxy)-2-hydroxy-propylamino]-ethyl]-*N*′-[4-(2-[^{18}F]fluoro-ethoxy)-phenyl]-urea (B).

2. Methods

2.1. Radiochemistry

(*S*)-*N*-[2-[3-(2-Cyano-phenoxy)-2-hydroxy-propylamino]-ethyl]-*N*′-[4-(2-[^{18}F]fluoro-ethoxy)-phenyl]-urea [(S)-[^{18}F]F-ICI)] was prepared by a two-step synthesis from ethylene glycol ditosylate, [^{18}F]fluoride ion and the phenol precursor, (*S*)-*N*-[2-[3-(2-cyano-phenoxy)-2-hydroxy-propylamino]-ethyl]-*N*′-(4-hydroxy-phenyl)-urea, as described elsewhere [24].

2.2. Pharmaceuticals

Unlabelled (*S*)-F-ICI was prepared as described previously [24]. It was dissolved in ethanol/dimethylsulphoxide (DMSO)/water (25/1/50, v/v/v) at 2 μmol·ml^{-1} for injection into animals.

The non-selective β-AR antagonists, propranolol HCl and CGP 12177 HCl, and the β_1-AR selective antagonist, CGP 20712A, were purchased from Sigma Aldrich Chemie (Germany). These antagonists were dissolved in saline at concentrations of 5 μmol·ml^{-1} for injection.

2.3. Animals

Studies were approved by local and federal ethics committees and were performed in accordance with institutional guidelines for health and care of experimental animals.

Male CD1 mice (30-40 g) or Wistar rats (270−430 g) which had free access to food were anaesthetised by inhalation (isoflurane 2%, oxygen 0.5 l·min^{-1}) for insertion of indwelling intravenous catheters. For PET scanning, each mouse or rat had a catheter in one lateral tail vein. For ex vivo biodistribution studies each rat had two catheters, one in the ventral tail artery and one in a lateral tail vein. Animals

were allowed to recover for 1–2 h under light restraint before being re-anaesthetised for PET scanning. Ex vivo biodistribution and metabolite studies were carried out with conscious animals [21,23,26].

2.4. PET scanning

PET was carried out using a sub-millimeter high resolution (0.7-mm full width at half maximum) dedicated small animal scanner (32 module quadHIDAC, Oxford Positron Systems, UK). This scanner uses wire-chamber detectors and offers uniform spatial resolution (<1 mm) over a large cylindrical field (165-mm diameter, 280-mm axial length) [27,28].

Two anaesthetised mice or rats (isoflurane 2%, oxygen 0.2 l·min^{-1} per mouse or 0.5 l·min^{-1} per rat) were placed on a heating pad to maintain body temperature during the scan. Animals were positioned on the scanner and 30 s after the start of data acquisition (*S*)-[^{18}F]F-ICI (1–3 MBq in 100 μl for mice or 4.8−8.7 MBq in 200 μl for rats) was injected simultaneously into each animal in the scanner via the tail vein catheters. For each scan, one animal was given unlabelled (*S*)-F-ICI (2 μmol·kg^{-1}) or the non-selective β-AR blocker propranolol (5 μmol·kg^{-1}) 15 min after injection of (*S*)-[^{18}F]F-ICI. To confirm the location of the heart, 2-[^{18}F]fluoro-2-deoxy-D-glucose ([^{18}F]FDG) (3–7.5 MBq in 50 μl for mice or 9 MBq in 200 μl for rats) was injected via the tail vein 5–10 min after completion of the (*S*)-[^{18}F]F-ICI scan and data were acquired for 30 min. To improve myocardial uptake of [^{18}F]FDG in rats, 0.5 ml glucose (20%) was injected 5 min before [^{18}F]FDG.

List-mode data were acquired for 60 min [(*S*)-[^{18}F]F-ICI] or 30 min ([^{18}F]FDG) and subsequently reconstructed using an iterative reconstruction algorithm [29]. PET images were analysed using in-house software programmes in MATLAB (The MathWorks Company) and C programming languages [28]. Details of the analysis are published elsewhere [23]. In brief, the total radioactivity in each animal was assessed by drawing a cube encompassing the body, excluding the tail and paws, on the reconstructed [^{18}F]FDG image (15−30 min time frame). The parameters defining this cube were saved and used to compute the whole body radioactivities (cps mouse or rat) for each frame of the (*S*)-[^{18}F]F-ICI scan. The parameters required to create images of each heart and to compute time-activity curves for (*S*)-[^{18}F]F-ICI were also defined using the [^{18}F]FDG scan. The average radioactivity in a given volume of interest (cps·ml^{-1}) was calculated for each time frame and expressed as a percentage of the whole body activity defined as:

$$\text{cps}\cdot\text{ml}^{-1}(\%\ \text{mouse or rat}) = 100 \times \frac{(\text{cps}\cdot\text{ml}^{-1})_{\text{myocardium}}}{(\text{cps})_{\text{whole body}}}$$

2.5. Ex vivo biodistribution studies

Ex vivo biodistribution studies were carried out in rats (as described previously [21,23,25]. (*S*)-[^{18}F]F-ICI or unlabelled antagonists were injected as a bolus (1 μl·g^{-1} body weight) via the tail vein. Aliquots of each (*S*)-[^{18}F]F-ICI injectate were diluted in ethanol/saline and measured to determine the radioactivity injected into each rat. Six sequential arterial blood samples (ca. 100 μl) were taken from some rats. Rats were sacrificed by intravenous injection of sodium pentobarbitone (Euthatal) at 200 mg·(kg body weight)$^{-1}$ at predetermined times after injection and tissues rapidly removed. Tissue radioactivity was measured by an automated gamma counter (Wallac Wizard 3, Perkin Elmer Life Sciences, Boston, MA, USA). Radioactivity was expressed as an uptake index, defined as:

$$\text{Uptake index} = \frac{\text{Tissue radioactivity (cpm)} / \text{Tissue wet weight (g)}}{\text{Radioactivity injected (cpm)} / \text{Body weight (g)}}$$

2.6. HPLC analysis of radiometabolites

Radiometabolites in plasma and urine were assessed by gradient RP-HPLC [23]. Rats (280–350 g) were injected with 20–110 MBq (140–300 nmol·kg^{-1}) (*S*)-[^{18}F]F-ICI via the tail vein catheters. Up to three blood samples (1 ml) were collected from the tail artery catheter at 2–25 min after injection of radioligand. Cell-free plasma was prepared by centrifuging each blood sample at 2000 g for 2 min. Ice-cold acetonitrile (0.7 ml) was added to the plasma (0.5 ml) and the precipitated proteins were removed by centrifugation. A sample of the resulting supernatant (200 μl) was spiked with non-radioactive (*S*)-F-ICI (10μg) for HPLC analysis using a gradient RP-HPLC system composed of two Knauer K-1800 pumps, a Knauer S-2500 UV detector, a Raytest Gabi Star γ-detector and a RP-HPLC Nucleosil Eurosphere 100-10 C-18 column (250×8 mm). The following conditions were applied: eluent A: water (0.1% TFA), eluent B: acetonitrile (0.1% TFA), gradient from 85% A to 30% A in 18 min, halt at 30% A for 5 min, gradient from 30% A to 85% A in 1 min, flow: 5.5 ml·min^{-1}. The eluate was monitored for radioactivity and UV absorbance (λ=254 nm).

3. Results

3.1. Radiochemistry

The specific activities of the [^{18}F]F-ICI used in this study, ranged from 0.8 to 16.9 GBq·μmol^{-1} (mean 4.7±1.8 GBq·μmol^{-1}, n=10) at the end of synthesis. These are lower than the value previously published (40±8 GBq/μmol) [24] because the activities of [^{18}F]fluoride at the start of radiosynthesis were lower than those used in the earlier paper. In our experience, the amount of carrier [^{19}F]fluoride that is introduced in our specific synthesis procedure, using our specific synthesiser, O-18-water and chemicals, is constant and independent of the [^{18}F]fluoride radioactivity at the start of synthesis. Consequently, the specific activity should be lower in this paper. Furthermore, the preparations were performed in a synthesiser with old TEFZEL (a

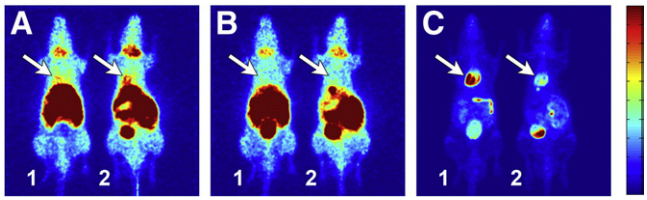

Fig. 2. Distribution of radioactivity in mice after intravenous injection of (*S*)-[^{18}F]F-ICI visualised by the quadHIDAC scanner. Two anaesthetised (isoflurane/oxygen) mice were placed in the scanner and (*S*)-[^{18}F]F-ICI (1.8 MBq per mouse in 100 μl, 5.5±0.2 nmol·kg^{-1}) was injected simultaneously into each. 20 min after (*S*)-[^{18}F]F-ICI, mouse 1 received vehicle (50 μl: ethanol/DMSO/water, 25/1/50, v/v/v) and mouse 2 unlabelled (*S*)-F-ICI (2 μmol·kg^{-1}, 50 μl). Both mice received [^{18}F]FDG (7.5 MBq per mouse in 50 μl) after the (*S*)-[^{18}F]ICI scan. The images show the mice lying on their fronts with their hearts to the left of the image. Data for 16 planes were summed to show the heart chambers. The arrows indicate the positions of the hearts. (A) 5–15 min after injection of (*S*)-[^{18}F]F-ICI. (B) 40–60 min after (*S*)-[^{18}F]F-ICI, i.e., 20–40 min after vehicle (mouse 1) or unlabelled (*S*)-[^{18}F]F-ICI (mouse 2). (C) 15–30 min after [^{18}F]FDG. Colour density scale: dark blue minimum (0 cps·ml^{-1}), dark red maximum (350 cps·ml^{-1} for (*S*)-[^{18}F]F-ICI or 5000 cps·ml^{-1} for [^{18}F]FDG).

fluoropolymer) tubes, which potentially increase the fluoride carrier and decrease the specific activity.

3.2. PET scanning of mice

Fig. 2 illustrates the biodistribution of radioactivity after intravenous injection of (*S*)-[^{18}F]F-ICI into mice. The hearts can be seen but there was high uptake of radioactivity in abdominal regions (liver, intestine, kidney, and bladder). Fig. 2 illustrates radioactivity in coronal planes encompassing the heart chambers but excluding most of the brain. Examination of more dorsal planes indicted that there was no appreciable uptake in brain. The heart was barely visible after the injection of vehicle or unlabelled (*S*)-F-ICI (Fig. 2B). The positions of the hearts were confirmed by the [^{18}F]FDG scan carried out after completion of the (*S*)-[^{18}F]F-ICI scan (Fig. 2C).

Fig. 3 shows coronal images of the thoraces of the mice. These images have been rotated in the sagittal plane so that the hearts are shown as in clinical studies, i.e. as if the mice were on their backs with their hearts on the right (Fig. 3A and D). As in Fig. 2, unlabelled (*S*)-F-ICI injected 20 min after (*S*)-[^{18}F]F-ICI had no obvious effect on the later images (Fig. 3B and E). One-minute time frames were reconstructed for the (*S*)-[^{18}F]F-ICI scan and time-activity curves were computed for regions of interest drawn round the left ventricle wall and septum. Myocardial radioactivity was detected immediately after injection and reached a maximum during the first minute. The early phase (<5min) of rapid loss from the left ventricle wall and septum was followed by a slow loss of myocardial radioactivity. Injection of unlabelled (*S*)-F-ICI had no significant effect on this loss.

3.3. PET scanning of rats

Fig. 4 illustrates the biodistribution of radioactivity after intravenous injection of (*S*)-[^{18}F]F-ICI into rats. As for mice, the hearts can be seen (Fig. 4A), and there was high uptake of radioactivity in liver, intestine, kidney, and bladder but little in brain. In Fig. 4, saline or the non-selective β-AR antagonist propranolol was injected at 20 min and in the rats neither heart was visible at late times (Fig. 4B). The positions of both hearts, however, were confirmed by the [^{18}F]FDG scan carried out after completion of the (*S*)-[^{18}F]F-ICI scan (Fig. 4C).

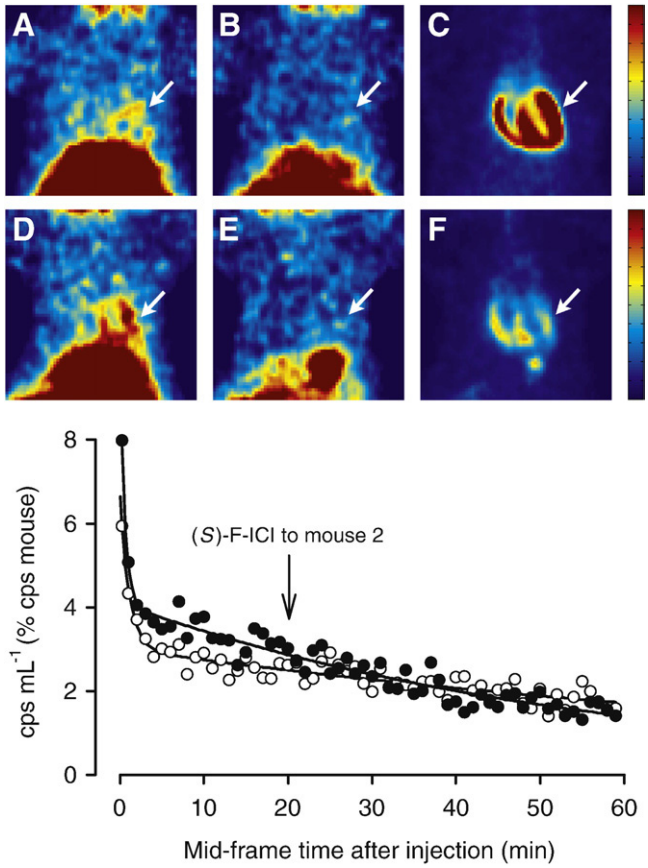

Fig. 3. Uptake of radioactivity in the mouse heart after intravenous injection of (*S*)-[^{18}F]F-ICI visualised by the quadHIDAC PET scanner. Two anaesthetised (isoflurane/oxygen) mice were placed in the scanner [(A–C) mouse 1; (D–F) mouse 2]. (S)-[^{18}F]F-ICI (1.8 MBq per mouse in 100 μl," 5.5±0.2 nmol·kg^{-1}) was injected simultaneously into each and the heart was visualised by summing eight myocardial planes at 5–15 min (A, D). The images show the mice lying on their backs, their hearts to the right of the image. The arrows indicate the positions of the hearts. 20 min after (*S*)-[^{18}F]ICI, mouse 1 received vehicle (100 μl: ethanol/DMSO/saline, 25/1/50, v/v) and mouse 2 unlabelled (*S*)-F-ICI (2 μmol·kg^{-1}, 50 μl). Myocardial images at 40–60 min were comparable (B, E). Both mice received [^{18}F]FDG (7.5 MBq per mouse in 50 μl) after the (*S*)-[^{18}F]F-ICI scan (C, F). Colour density scale: dark blue minimum (70 cps·ml^{-1}), dark red maximum (350 cps·ml^{-1} for (*S*)-[^{18}F]F-ICI or 5000 cps·ml^{-1} for [^{18}F]FDG). Time activity curves were computed for (*S*)-[^{18}F]F-ICI (see text). ○ vehicle; ● unlabelled (*S*)-F-ICI.

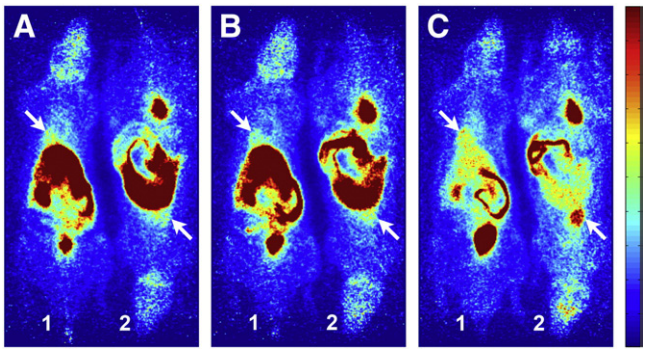

Fig. 4. Distribution of radioactivity in rats after intravenous injection of (*S*)-[^{18}F]F-ICI visualised by the quadHIDAC scanner. Two anaesthetised (isoflurane/oxygen) rats were placed in the scanner and (*S*)- [^{18}F]F-ICI (4.8 MBq per rat in 100 µl, 2.9 nmol·kg^{-1}) was injected simultaneously into each. 20 min after (*S*)-[^{18}F]F-ICI, rat 1 received unlabelled propranolol (5 µmol·kg^{-1}, 200 µl) and rat 2 vehicle (saline). Both rats received [^{18}F]FDG (9 MBq per rat in 100 µl) after the (*S*)-[^{18}F]F-ICI scan. The images show the rats lying on their fronts, rat 1 head in scanner with its heart to the left, rat 2 tail in scanner with its heart to the right of the image. Data for 18 planes were summed to show the heart chambers. The arrows indicate the positions of the hearts. (A) 5–15 min after injection of (*S*)-[^{18}F]F-ICI. (B) 40–60 min after (*S*)-[^{18}F]F-ICI, i.e., 20–40 min after propranolol (rat 1) or vehicle (rat 2). (C) 15–30 min after [^{18}F]FDG. Colour density scale: dark blue minimum (0 cps·ml^{-1}), dark red maximum (50 cps·ml^{-1} for (*S*)-[^{18}F]F-ICI or 100 cps·ml^{-1} for [^{18}F]FDG).

Fig. 5 shows coronal images of the thoraces of the rats shown in Fig. 4. Again, the hearts are shown as in clinical studies, i.e., as if the rats were on their backs with their hearts on the right (Fig. 5A and D). Propranolol had no visible effect (Fig. 5B and E). Time-activity curves were similar to those for mice. Myocardial radioactivity cleared rapidly during the first 5 min to a low level and injection of propranolol at 20 min had no significant effect on the slow phase of loss.

The nanomolar doses of (*S*)-F-ICI injected for PET scanning ranged from 3–10 (data not shown) nmol·kg^{-1}. Unlabelled (*S*)-F-ICI in the dispensed material competes with radioactively labelled (*S*)-[^{18}F]F-ICI for any binding sites and these doses may preclude the detection of specific binding by PET. Lower amounts of radioactivity can be used for ex vivo studies which use well-counter gamma detection techniques.

3.4. Ex vivo biodistribution in rats

Clearance of radioactivity from plasma after intravenous injection of (*S*)-[^{18}F]F-ICI is shown in Fig. 6. There was a rapid loss of plasma radioactivity during the first 5 min after radiotracer injection, followed by a slow clearance. Comparable results were obtained for injected doses ranging from 0.5 to 8 nmol·kg^{-1}. Data for all doses, therefore, were combined and a single biexponential fit is shown in Fig. 6.

Fig. 7 illustrates uptake of radioactivity in various tissues as a function of time after injection of (*S*)-[^{18}F]F-ICI at doses ranging from 0.5 to 8 nmol·kg^{-1}. In all tissues, maximum radioactivity was observed at the first dissection time (2 min). The very high uptake observed for kidney at 2 min (UI 25, equivalent to 8.4 cpm·g^{-1} % injected cpm for a 300 g rat) decreased exponentially (at 30 min UI=1.9, cpm·g^{-1} % injected cpm=0.64), consistent with rapid clearance by the kidneys. After the initial peaks, radioactivity cleared more slowly from other tissues. For example, at 30 min after injection, uptake indices for liver and heart were 3.9 and 1.7 (1.3 and 0.56 cpm·g^{-1} % injected cpm), respectively, compared to 0.53 (0.18, % injected·g^{-1}) for plasma. Similar results were obtained for low (0.5–1 nmol·kg^{-1}) and high (8 nmol·kg^{-1}) nanomolar doses. Radioactivity was detected in the urine at all times after injection of tracer (data not shown).

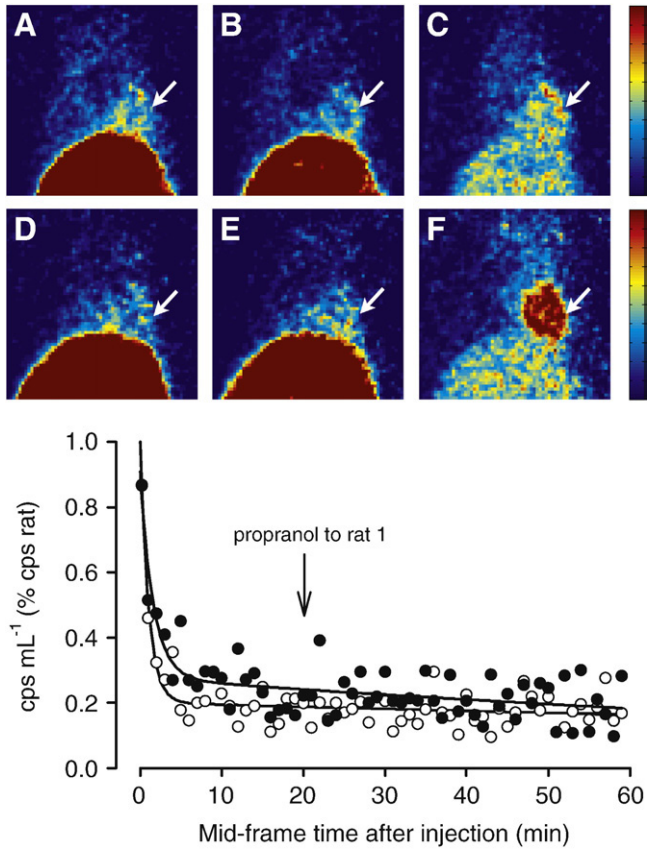

Fig. 5. Uptake of radioactivity in the rat heart after intravenous injection of (*S*)-[^{18}F]F-ICI visualised by the quadHIDAC PET scanner. Two anaesthetised (isoflurane/oxygen) rats were placed in the scanner [(A–C) rat 1; (D–F) rat 2]. (S)-[^{18}F]F-ICI (4.8 MBq per rat in 100 µl, 2.9 nmol·kg^{-1}) was injected simultaneously into each and the heart was visualised by summing 12 myocardial planes at 5–15 min (A, D). The images show the rats lying on their backs, their hearts to the right of the image. The arrows indicate the positions of the hearts. 20 min after (*S*)-[^{18}F]F-ICI, rat 1 received propranolol (5 µmol·kg^{-1}, 200 µl) and rat 2 vehicle (200 µl, saline). Myocardial images at 40–60 min were comparable (B, E). Both rats received [^{18}F]FDG (9 MBq per rat in 100 µl) after the (*S*)-[^{18}F]F-ICI scan (C, F). Colour density scale: dark blue minimum (10 cps·ml^{-1} for (*S*)-[^{18}F]F-ICI or 20 cps·ml^{-1} for [^{18}F]FDG), dark red maximum (50 cps·ml^{-1} for (S)-[^{18}F]F-ICI or 100 cps·ml^{-1} for [^{18}F]FDG). Time activity curves were computed for (S)-[^{18}F]F-ICI (see text). ○ vehicle; ● propranolol.

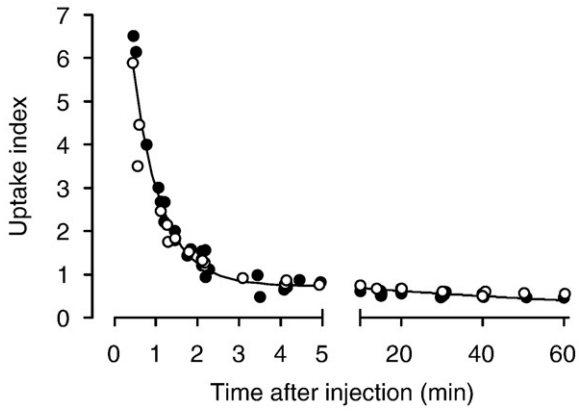

Fig. 6. Clearance of radioactivity from plasma of rats (260–340 g) after intravenous injection of (S)-[^{18}F]F-ICI. (*S*)-[^{18}F]F-ICI (0.08–4 MBq·kg^{-1}) was injected intravenously, and one to six arterial samples were taken from each rat (n=22). Nanomolar doses were 0.5–2 nmol·kg^{-1} (14 rats) (●), 5–8 nmol·kg^{-1} (eight rats) (○). The line is the bi-exponential fit for radioactivity versus time for all data points.

Two experiments (12 rats) were carried out to compare the effects of predosing with the β_1-AR selective antagonist CGP 20712A to those of the non-selective antagonist propranolol. Fig. 8 shows the results with data from the time activity study (Fig. 7, 30 min, 0.5 and 1.0 nmol·kg^{-1}) used for the case designated as (*S*)-[^{18}F]F-ICI given alone. Uptake indices for heart and lung were significantly higher in rats which received vehicle before (*S*)-[^{18}F]F-ICI than in those without pretreatment (t test, df=4, P<.05). When compared to vehicle controls, there was a small but significant reduction in radioactivity in myocardium and lung after predosing with CGP 20712A or propranolol (t test, df=5, P<.02) but not in the other tissues studied. When compared to (*S*)-[^{18}F]F-ICI alone, however, the reduction was only significant in lung after CGP 20712 A (t test, df=5; P<.02).

The results shown in Figs. 7 and 8 suggest that myocardial uptake of (*S*)-[^{18}F]F-ICI radioactivity does not depend on injected dose (>0.5 nmol·kg^{-1}). In vitro competition studies, however, indicate a very high affinity of (*S*)-F-ICI for β_1-ARs which may compromise detection of specific binding by PET. The effect of injected dose, therefore, was investigated by injecting serial dilutions of dispensed (*S*)-[^{18}F]F-ICI and assessing tissue radioactivity at 30 min after injection. There was a linear relationship between myocardial uptake, expressed as cpm·(g wet tissue)$^{-1}$, and injected radioactivity [cpm·(g body weight)$^{-1}$] which was independent of the specific activity of the dispensed (*S*)-[^{18}F]F-ICI (0.8 or 2.5 GBq·μmol^{-1}). In other words, the uptake index was not dependent on injected dose between 0.04 and 200 nmol·kg^{-1} (Fig. 9). Similar results were obtained for other tissues (e.g., liver and plasma in Fig. 9).

Radioligands which have proved useful for studying myocardial neuroreceptors by PET show a decrease in myocardial uptake index as the dose of injected ligand is increased [21,26,30,31]. In vivo dose effect curves for the non-selective β-AR radioligand (*S*)-[^{3}H]CGP 12177 have been published for rat myocardium, giving a "B_{max}" of 4.7 pmol·(g myocardium)$^{-1}$ and a "K_D" of 0.58 nmol·(kg body weight)$^{-1}$ [21]. Using these values to calculate myocardial uptake of CGP 12177 as a function of injected dose gives the dotted line shown in Fig. 9. For CGP 12177 "non specific" uptake (injected dose >10 nmol·kg^{-1}) was ~1 and as injected dose was decreased the uptake index increased to >5 at <0.5 nmol·kg^{-1}. Uptake indices for (*S*)-

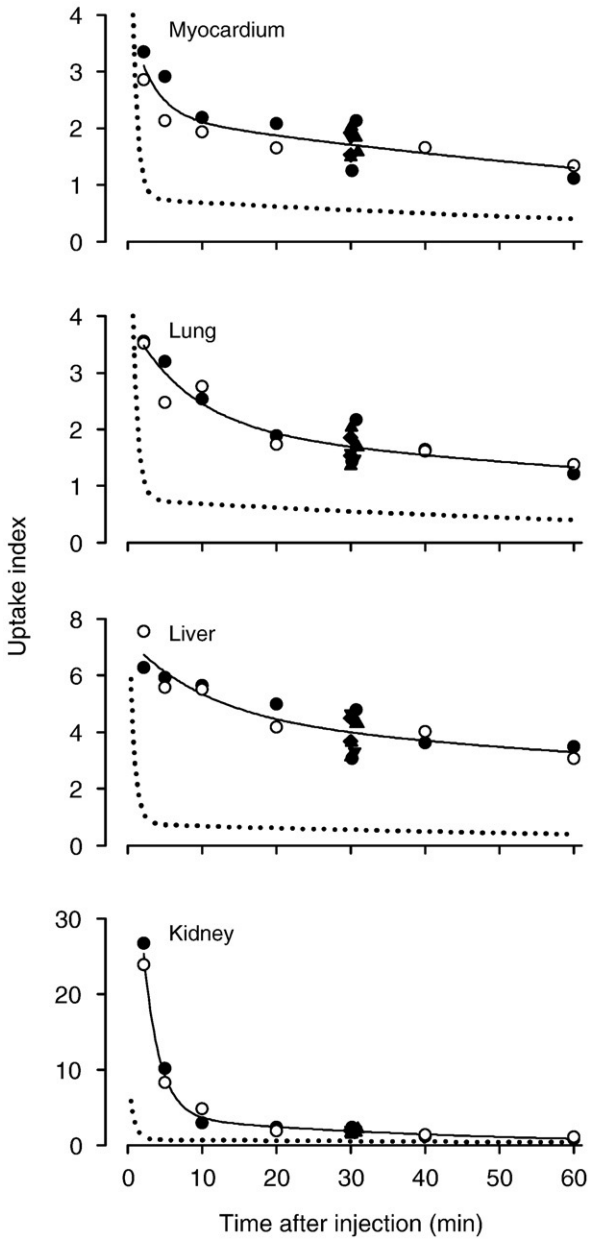

Fig. 7. Radioactivity in tissues of rats (260–340 g) after intravenous injection of (*S*)-[^{18}F]F-ICI (0.08–4 MBq·kg^{-1}). Each symbol indicates an uptake index for one rat. Nanomolar doses were 0.5 nmol·kg^{-1} (▲), 1 nmol·kg^{-1} (●), 2 nmol·kg^{-1} (▼), 5 nmol·kg^{-1} (♦), or 8 nmol·kg^{-1} (○). The solid line for each tissue is the bi-exponential fit to data for all doses. The dotted line is the exponential fit to plasma radioactivity shown in Fig. 6.

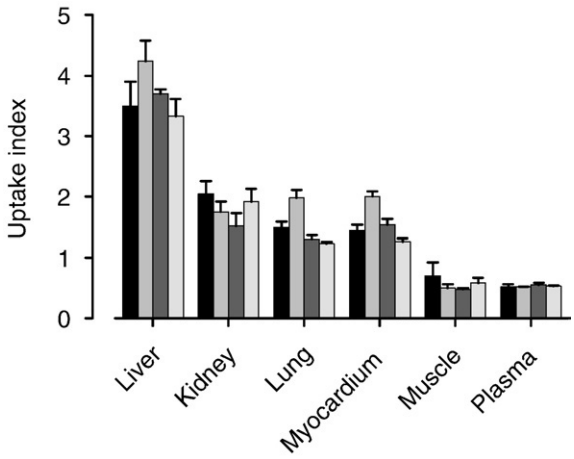

Fig. 8. Biodistribution of radioactivity in tissues of rats 30 min after intravenous injection of (*S*)-[^{18}F]F-ICI (0.082–1.62 MBq·kg^{-1}, 0.5–1.0 nmol·kg^{-1}). Bars indicate average values for uptake indices and standard errors are shown. (*S*)-[^{18}F]F-ICI was given alone (three rats) (■) or 5 min after vehicle (three rats) (■), CGP 20712A at 5 μmol·kg^{-1} (four rats) (■) or propranolol at 5 μmol·kg^{-1} (four rats) (■).

[^{18}F]F-ICI were 2 at comparable doses, consistent with nonspecific binding of radioligand.

3.5. Radiometabolites

Fig. 10 shows HPLC analyses of samples of plasma and urine taken after intravenous injection of (*S*)-[^{18}F]F-ICI into three rats studied on different days. (*S*)-[^{18}F]F- ICI eluted at 11 min. (*S*)-[^{18}F]F-ICI and metabolites at ~2 min and possibly 9 min were detected in plasma at early times (2.5 and 5 min after injection) but only polar metabolites were

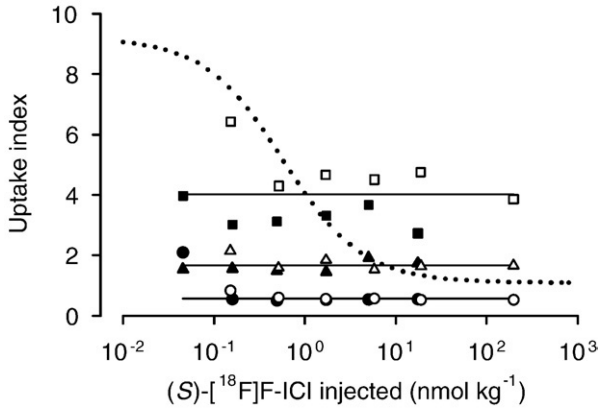

Fig. 9. Uptake of radioactivity in tissues of rats 30 min after intravenous injection of (*S*)-[^{18}F]F-ICI as a function of injected dose. Serial dilutions of dispensed (*S*)-[^{18}F]F-ICI (specific activity at dispense 0.8 (■●▲) or 2.4 (□○△) GBq·μmol^{-1}) were made for injection. Each symbol indicates an uptake index for one rat. Data for liver (■ □), myocardium (▲ △) and plasma (● ○) are shown. The solid lines shows the average values for each tissue. The dotted line shows the relationship between uptake index and injected dose for the nonselective β-AR ligand CGP 12177 in rat myocardium [21].

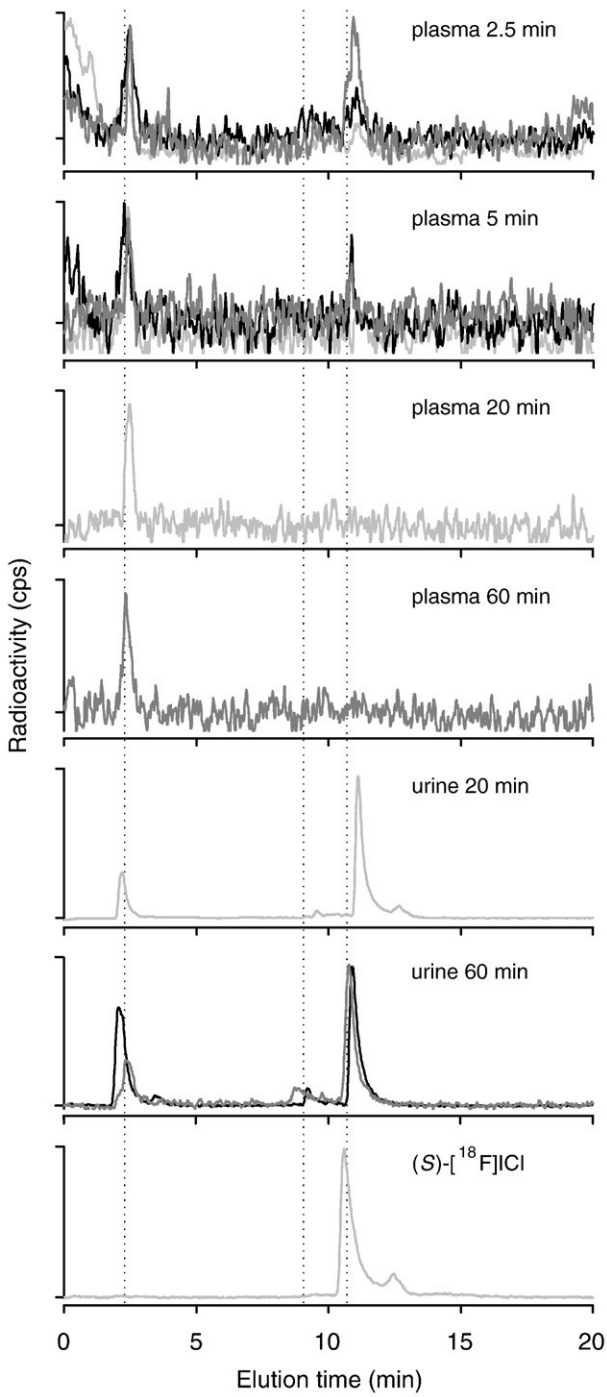

Fig. 10. HPLC traces for samples of plasma and urine taken after intravenous injection of (*S*)-[^{18}F]F-ICI in rats. In each panel radioactivity, corrected for background, (cps) is plotted against elution time. Results for 3 rats studied on different days are superimposed (rat 1, 21 MBq, ~100 nmol·kg^{-1} ——; rat 2, 44 MBq, ~320 nmol·kg^{-1} ——; rat 3, 111 MBq, 140 nmol·kg^{-1} ——). The HPLC trace for a sample of the injectate used for Rat 3 is shown in the bottom panel (see text). Vertical broken lines indicate elution tímes for (*S*)-[^{18}F]F-ICI (11 min) and possible metabolites (2 and 9 min).

seen later (20 and 60 min after injection). On the third day, the radiochemical purity of the synthesised (*S*)-[^{18}F]F-ICI was poor (88%) compared with the usual value (>95%) and

the HPLC trace for the injectate given to Rat 3 is shown in Fig. 10. The impurity (~12 min) was not detectable in the plasma (2.5, 5 and 20 min) but was seen in the urine (20 min) together with parent (*S*)-[^{18}F]F-ICI and polar metabolites. Both (*S*)-[^{18}F]F-ICI and polar metabolites were detected in urine at 60 min after injection.

4. Discussion

The heart was clearly visible in quadHIDAC PET scans of both mice (Fig. 2) and rats (Fig. 4) following intravenous injection of (*S*)-[^{18}F]F-ICI. The apparent loss of myocardial radioactivity observed during 0.5–5 min (Figs. 3 and 5), is due to a combination of decreases in radioactivity in the myocardial microcirculation and of reduced spillover as radioactivity in the heart chambers decreases. After vascular mixing and the initial rapid phase of loss, a higher proportion of the injected (*S*)-[^{18}F]F-ICI radioactivity was observed in the myocardium of mice (2–3 cps·ml^{-1} % mouse, Fig. 3) than of rats (0.1-0.3 cps·ml^{-1} % rat, Fig. 5). Myocardial uptake of radioactivity, however, was low compared to the uptake of radioactivity in liver, kidney and bladder. There was a low level of radioactivity in the brain in both mice and rats, an observation which is consistent with the low lipophilicity of F-ICI (logP=1.44, log D=0.17) [24], similar to that of the parent compound ICI 89,406 (logP=1.57, logD=0.13) [17]. Injection of unlabelled (*S*)-F-ICI (2 μmol·kg^{-1}) (Fig. 3) or propranolol (5 μmol·kg^{-1}) (Fig. 5) at 20 min had no effect on the rate of loss of radioactivity from the myocardium.

To demonstrate specific binding of a radioligand to a receptor by predosing or displacement using unlabelled ligands, the amount of radioligand used should give low levels of receptor occupancy (<1%) [30]. It may not be possible to achieve the specific activity required to allow the injection of sufficient radioactivity to acquire statistically significant PET data while maintaining low receptor occupancy in small animals. If the radioactivity required for PET is equivalent to a ligand dose which saturates the receptor of interest, it will not be possible to demonstrate specific receptor binding using PET.

The doses of (*S*)-[^{18}F]F-ICI used in the PET studies were 6 nmol·kg^{-1} for mice and 3 nmol·kg^{-1} for rats. For the non-selective β-AR ligand (*S*)-[^{3}H]CGP 12177 injected intravenously into rats, a dose of 3 nmol·kg^{-1} reduced myocardial "specific" uptake of radioactivity to 20% of that observed for 1 nmol and 15 nmol·kg^{-1} completely blocked it [25]. Using current ^{18}F-labelling methods, the dispensed solution of (*S*)-[^{18}F]F-ICI includes unlabelled (*S*)-F-ICI. The 3–6 nmol·kg^{-1} used in the PET scan may give an in vivo occupancy by unlabelled (*S*)-F-ICI which is too high for the detection of specific binding of (*S*)-[^{18}F]F-ICI to β_1-AR by predosing or displacement experiments.

Lower doses of (*S*)-[^{18}F]F-ICI (<1 nmol·kg^{-1}) could be used in the ex vivo dissection studies. These studies showed that after vascular mixing (0–30 s), plasma radioactivity decreased to ~10% during the first 5 min after injection of (*S*)-[^{18}F]F-ICI (Fig. 6). In all tissues studied, maximum radioactivity was observed at the first dissection time (2 min). After the initial peaks, radioactivity cleared more slowly from tissues than from plasma, consistent with a small uptake in extravascular compartments. Radioactivity in the kidney was especially high immediately after injection; subsequently, there was a rapid exponential loss consistent with high kidney extraction of the tracer. Similar results were obtained for low (0.5–1 nmol·kg^{-1}) and high (8 nmol·kg^{-1}) nanomolar doses suggesting that either there was no specific uptake or that the in vivo "K_i" was ≪ 0.5 nmol·kg^{-1}.

The ex vivo biodistribution studies, however, failed to demonstrate high specific binding using low doses of (*S*)-[^{18F}]F-ICI (0.5–1.0 nmol·kg^{-1}). Although predosing with the selective β_1-AR antagonist CGP 20712A or the non-selective antagonist propranolol at high dose (5 μmol·kg^{-1}) had small effects on myocardial and lung radioactivity (Fig. 8), whether or not these differences are physiologically relevant is uncertain. When compared to vehicle controls, there was a small but statistically significant reduction in radioactivity in myocardium and lung after predosing with CGP 20712A or propranolol (*t* test, *df*=5, *P*<.02) but when compared to (*S*)-[^{18}F]F-ICI alone, the reduction was only significant in lung after CGP 20712 A (*t* test, *df*=5, *P*<.02). Considering the different β_1 to β_2 ratios in myocardium (β_1>β_2) and lung (β_2>β_1) [33], CGP 20712A might be expected to have the greater effect in myocardium. Moreover, radioactivity in plasma was not effected by the nanomolar dose of (*S*)-F-ICI (Fig. 6) or by predosing (Fig. 8), whereas increases are observed after β-AR blockade for β-AR radioligands such as CGP12177 [26] and fluorocarazol [30].

Injected doses >0.5 nmol·kg^{-1} may include sufficient unlabelled (*S*)-F-ICI to reduce the proportion of (*S*)-[^{18}F]F-ICI bound to β_1-AR to undetectable levels. Reducing injected (*S*)-[^{18}F]F-ICI to 0.04 nmol·kg^{-1}, however, did not increase the percentage of the injected radioactivity taken up by the myocardium. There was a linear relationship between myocardial uptake, expressed as cpm·(g wet tissue)$^{-1}$, and injected radioactivity expressed as cpm·(g body weight)$^{-1}$. Consequently, the uptake index was not dependent on injected dose between 0.04 and 200 nmol·kg^{-1} (Fig. 9). Similar results were obtained for other tissues (eg, liver and plasma) in which specific binding to β_1-AR was not expected. A radioligand specific for β-AR, for example. (*S*)-CGP 12177, with an ex vivo K_i of 0.58 nmol·(kg body weight)$^{-1}$ [21], would give a sigmoidal dose effect curve (Fig. 9). For (*S*)-[^{3}H]CGP-12177 "non-specific" uptake (injected dose >10 nmol·kg^{-1}) was ~1, and as injected nanomolar dose was decreased, the uptake index increased to >5 at <0.5 nmol·kg^{-1}. Comparable dose effect curves have been reported for the β_2-AR selective radioligand (*S*)-1′-[^{18}F]fluorocarazol [30]. Uptake indices for doses >10 nmol·kg^{-1} were ~0.5 whereas that for 0.5 nmol·kg^{-1}

was ~2.2. For a subtype selective ligand, the uptake index at low doses would depend on the relative numbers of each subtype. For rat myocardium, 50–80% of β-ARs are of the β_1-subtype [31–37] from which it might be expected that the uptake index at 0.5 nmol·kg^{-1} would be 3–4 for the β_1-subtype and 1–2 for the β_2-subtype. Uptake indices for (*S*)-[^{18}F]F-ICI were 2 for a wide range of doses (Fig. 9), consistent with no specific binding to β-ARs.

For the non-selective β-AR ligand (*S*)-[^{11}C]CGP 12177 in rats, a dose of 0.58 nmol·kg^{-1} halved myocardial uptake [21]. In vitro membrane binding studies show that the K_D for CGP 12177 (0.19−0.67 nM [34–38]) is 4–14 times greater than the K_i for (*S*)-F-ICI (0.049 nM [24]). If metabolism were similar, radioligands with higher affinity to β_1-AR would be expected to give sigmoid dose effect curves shifted to lower doses (in vivo $K_i \ll 0.5$ mol·(kg body weight)$^{-1}$ with higher uptake indices at low doses. Considered together, Figs. 3, 5, 8, 9 indicate that there is no detectable specific binding of (*S*)-[^{18}F]F-ICI to β_1-ARs.

The HPLC studies showed rapid breakdown of (*S*)-[^{18}F]F-ICI (Fig. 10). (*S*)-[^{18}F]F-ICI and polar metabolites were detected in plasma at early times (2.5 and 5 min) but only polar metabolites were seen later (20 and 60 min). Both (*S*)-[^{18}F]F-ICI and polar metabolites were detected at 20 and 60 min in urine. Rapid metabolism and excretion of (*S*)-[^{18}F]F-ICI would result in a low availability of radioligand to myocytes and consequently a very low occupancy of myocardial β_1-AR which precludes the detection of specific binding by dissection techniques. An alternative explanation for the failure to demonstrate an effect of predosing with unlabelled antagonists could be that labelled metabolites rather than parent compound were present in myocardium. Studies to assess radioactive metabolites in myocardium were not carried out as myocardial radioactivity at later times after injection, when radioactivity had cleared form the blood, was below detection by HPLC. The nonspecific binding observed in the blocking studies, however, is greater than that observed for the hydrophilic non-subtype-selective ligand CGP 12177, suggesting that (*S*)-F-ICI has a higher non-specific binding to myocardial membranes.

The biodistribution, low myocardial uptake and failure to demonstrate specific binding of [^{18}F]F-ICI to myocardial β_1-ARs are comparable to the results for [^{11}C]ICI-OMe. The HPLC profiles of radioactive metabolites, however, differed. Two polar radioactive metabolites were observed in plasma after injection of [^{11}C]ICI-OMe [23], whereas only one was observed after [^{18}F]F-ICI. $^{11}CO_2$ was observed in exhaled air after [^{11}C]ICI-OMe [23]. Parent compound was detected in urine after injection of either derivative but radioactive metabolites in urine were only detected after [^{18}F]F-ICI. Unfortunately, both derivatives were rapidly metabolised and excreted.

Other novel compounds have been considered for radiolabelling. The β-AR antagonist, (*R*)-2-(2-hydroxy-3-(isopropylamino)propoxy)benzonitrile [39] is amenable to labelling with fluorine-18. We have synthesised this compound and have developed a fluorination method, based on a published procedure [40], in which the hydroxyl group is replaced by [^{18}F]fluoride. Unfortunately, the fluorinated derivative is unstable [41]. Derivatives of the lead structure LK204545 [42], that represents a β_1-selective AR ligand, are other candidates for labelling with fluorine-18. Work is underway to synthesize these compounds and to develop labelling methods.

5. Conclusions

A fluoroethoxy derivative of the β_1-adrenoceptor antagonist ICI 89,406 was labelled with fluorine-18 [(*S*)-[^{18}F]F-ICI]. Although in vitro membrane studies showed that (*S*)-F-ICI has high affinity and selectivity for β_1-ARs, the present study in mice and rats failed to demonstrate high specific binding of (*S*)-[^{18}F]F-ICI to myocardial β_1-AR following intravenous injection. Similar results were previously obtained for three other derivatives of ICI 89,406. New lead compounds for a β_1-selective AR radioligand for PET are, therefore, being investigated.

Acknowledgments

This work was supported by grants from the Deutsche Forschungsgemeinschaft (DFG), Sonderforschungsbereich 656 MoBil Münster, Germany (projects A5 and C6), by the Interdisciplinary Clinical Research Centre, Münster (IZKF, core unit SmAP), Germany, and by the EC - FP6-project DiMI (WP 11.1), LSHB-CT-2005-512146. Dr. V.W. Pike is supported by the Intramural Research Program of the National Institutes of Health (the National Institute of Mental Health), USA.

The authors would like to thank Dr. Klaus Schäfers for advice on HIDAC scanning and software for image analysis and Ms Christine Bätza, Mr Daniel Burkert, Ms Irmgard Hoppe and Ms Sandra Schröer for technical assistance.

References

[1] Molenaar P, Parsonage WA. Fundamental considerations of β-adrenoceptor subtypes in human heart failure. Trends Pharmacol Sci 2005;26:368–75.

[2] Brodde O-E, Bruck H, Leineweber K. Cardiac adrenoceptors: physiological and pathophysiological relevance. J Pharmacol Sci 2006;100:323–37.

[3] Lohse MJ, Engelhardt S, Eschenhagen T. What is the role of β-adrenergic signaling in heart failure? Circ Res 2003;93:896–906.

[4] Khamssi M, Brodde OE. The role of cardiac β_1- and β_2-adrenoceptor stimulation in heart failure. J Cardiovasc Pharmacol 1990;16(Suppl 5): S133–7.

[5] Steinfath M, Geertz B, Schmitz W, Scholz H, Haverich A, Breil I, et al. Distinct downregulation of cardiac β_1 and β_2 adrenoceptors in different human heart diseases. Naunyn-Schmiedeberg's Arch Pharmacol 1991;343:217–20.

[6] Steinfath M, Lavicky J, Schmitz W, Scholz H, Döring V, Kalmár P. Regional distribution of β_1- and β_2-adrenoceptors in the failing and nonfailing human heart. Eur J Clin Pharmacol 1992;42:607–11.

[7] Steinfath M, Lavicky J, Schmitz W, Scholz H, Döring V, Kalmar P. Changes in cardiac β-adrenoceptors in human heart diseases: relationship to the degree of heart failure and further evidence for etiology-related regulation of β_1 and β_2 subtypes. J Cardiothorac Vasc Anesth 1993;7:668–73.

[8] Brodde O-E, Zerkowski HR, Doetsch N, Motomura S, Khamssi M, Michel MC. Myocardial β-adrenoceptor changes in heart failure: concomitant reduction in β_1- and β_2-adrenoceptor function related to the degree of heart failure in patients with mitral valve disease. J Am Coll Cardiol 1989;14:323–31.

[9] Leineweber K, Büscher R, Bruck H, Brodde D-E. β-adrenoceptor polymorphisms. Naunyn-Schmiedeberg's Arch Pharmacol 2004;369:1–22.

[10] Schäfers M, Dutka D, Rhodes CG, Lammertsma AA, Hermansen F, Schober O, et al. Myocardial presynaptic and postsynaptic autonomic dysfunction in hypertrophic cardiomyopathy. Circ Res 1998;82:57–62.

[11] Schäfers M, Lerch H, Wichter T, Rhodes CG, Lammertsma AA, Borggrefe M, et al. Cardiac sympathetic innervation in patients with idiopathic right ventricular outflow tract tachycardia. J Am Coll Cardiol 1998;32:181–6.

[12] Wichter T, Schäfers M, Rhodes CG, Borggrefe M, Lerch H, Lammertsma AA, et al. Abnormalities of cardiac sympathetic innervation in arrhythmogenic right ventricular cardiomyopathy: quantitative assessment of presynaptic norepinephrine reuptake and postsynaptic β-adrenergic receptor density with positron emission tomography. Circulation 2000;101:1552–8.

[13] Kies P, Wichter T, Schäfers M, Paul M, Schäfers KP, Eckardt L, et al. Abnormal myocardial presynaptic norepinephrine recycling in patients with the Brugada syndrome. Circulation 2004;110:3017–22.

[14] de Jong RM, Willemsen ATM, Slart RHJA, Blanksma PK, van Waarde A, Cornel JH, et al. Myocardial β-adrenoceptor down-regulation in idiopathic dilated cardiomyopathy measured in vivo with PET using the new radioligand (S)-[^{11}C]CGP12388. Eur J Nucl Med Mol Imaging 2005;32:443–7.

[15] van Waarde A, Maas B, Doze P, Slart RH, Frijlink HW, Vaalburg W, et al. Positron emission tomography studies of human airways using an inhaled β-adrenoceptor antagonist, S-^{11}C-CGP 12388. Chest 2005;128:3020–7.

[16] Kopka K, Law MP, Breyholz HJ, Faust A, Höltke C, Riemann B, Schober O, et al. Non-invasive molecular imaging of β-adrenoceptors in vivo: perspectives for PET-radioligands. Curr Med Chem 2005;12:2057–74.

[17] Imperial Chemical Industries Limited, London (UK), Patent CH 605666 1978; DE 2458908 1975. Chem Abstr 1976; 84:43599.

[18] Majid PA, Schreuder JE, de Feyter PJ, Roos JP. Clinical, electrocardiographic, and hemodynamic effects of ICI 89,406, a new cardioselective β-adrenoceptor antagonist with intrinsic sympathomimetic activity, in patients with angina pectoris. J Cardiovasc Pharmacol 1980;2:435–44.

[19] Svendsen TL, Hartling O, Trap-Jensen J. Immediate haemodynamic effects of propranolol, practolol, pindolol, atenolol and ICI 89,406 in healthy volunteers. Eur J Clin Pharmacol 1979;15:223–8.

[20] Kopka K, Wagner S, Riemann B, Law MP, Puke C, Luthra SK, et al. Design of new β_1-selective adrenoceptor ligands as potential radioligands for in vivo imaging. Bioorg Med Chem 2003;11:3513–27.

[21] Riemann B, Law MP, Kopka K, Wagner S, Luthra SK, Pike VW, et al. High non-specific binding of the β_1-selective radioligand 2-[^{125}I]-ICI-H. Nuklearmedizin 2003;42:173–80.

[22] Wagner S, Kopka K, Law MP, Riemann B, Pike VW, Schober O, et al. Synthesis and first in vivo evaluation of new selective high affinity -adrenoceptor radioligands for SPECT based on ICI 89,406. Bioorg Med Chem 2004;12:4117–32.

[23] Law MP, Wagner S, Kopka K, Pike VW, Schober O, Schäfers M. Are [O-methyl-^{11}C]derivatives of ICI 89,406 β_1-adrenoceptor selective radioligands suitable for PET? Eur J Nucl Med Mol Imaging 2008;35:174–85.

[24] Wagner S, Law MP, Riemann B, Pike VW, Breyholz HJ, Höltke C, et al. Synthesis of an ^{18}F-labelled high affinity β_1-adrenoceptor PET radioligand based on ICI 89,406. J Label Compd Radiopharm 2006;49:177–95.

[25] Wagner S, Law MP, Riemann B, Pike VW, Breyholz HJ, Höltke C, et al. Synthesis of (*R*)- an (*S*)-[*O-methyl*-^{11}C]*N*-[2-[3-(2-cyanophenoxy)-2-hydroxy-propylamino]-ethyl]-*N*′-(4-methoxy-phenyl)-urea as candidate high affinity β_1-adrenoceptor PET radioligands. J Label Compd Radiopharm 2005;48:721–33.

[26] Law MP. Demonstration of the suitability of CGP 12177 for *in vivo* studies of β-adrenoceptors. Brit J Pharmacol 1993;109:1101–9.

[27] Jeavons AP, Chandler RA, Deuttman CAR. A 3D HIDAC-PET camera with sub-millimeter resolution for imaging small animals. IEEE Trans Nucl Sci 1999;3:468–73.

[28] Schäfers KP, Reader AJ, Kriens M, Knoess C, Schober O, Schäfers M. Performance Evaluation of the 32-module quadHIDAC small animal PET scanner. J Nucl Med 2005;46:996-1004.

[29] Reader AJ, Ally S, Bakatselos F, Manavaki R, Walledge RJ, Jeavons AP, et al. One-pass list-mode EM algorithm for high resolution 3D PET image reconstruction into large arrays. IEEE Trans Nucl Sci 2002;49:693–9.

[30] Doze P, Van Waarde A, Elsinga PH, Van-Loenen Weemaes AMA, Willemsen ATM, Vaalburg W. Validation of *S*-1′-[^{18}F]fluorocarazolol for in vivo imaging and quantification of cerebral beta-adrenoceptors. Eur J Pharmacol 1998;353:215–26.

[31] Law MP, Osman O, Pike VW, Davenport RJ, Cunningham VJ, Rimoldi O, et al. Evaluation of [^{11}C]GB67, a novel radioligand for imaging myocardial α_1-adrenoceptors with positron emission tomography. Eur J Nucl Med 2000;27:7–17.

[32] Hume SP, Gunn RN, Jones T. Pharmacological constraints associated with positron emission tomographic scanning of small laboratory animals. Eur J Nucl Med 1988;25:173–6.

[33] Minneman KP, Hegstrand LR, Molinoff PB. Simultaneous determination of *beta*-1 and *beta*-2-adrenergic Receptors in tissues containing both receptor subtypes. Mol Pharmacol 1979;16:34–46.

[34] Nanoff C, Freissmuth M, Schütz W. The role of a low β_1-adrenoceptor selectivity of [^{3}H]CGP-12177 for resolving subtype-selectivity of competitive ligands. Naunyn-Schmiedeberg's Arch Pharmacol 1987;336:519–25.

[35] Mysliveček J, Říčný J, Kolář F, Tuček S. The effects of hydrocortisone on rat heart muscarinic and adrenergic α_1, β_1 and β_2 receptors, propranolol-resistant binding sites and on some subsequent steps in intracellular signalling. Naunyn-Schmiedeberg's Arch Pharmacol 2003;368:366–76.

[36] Mysliveček J, Nováková M, Palkovits M, Križanoyá O, Kvetňanský R. Distribution of mRNA and binding sites of adrenoceptors and muscarinic receptors in the rat heart. Life Sci 2006;79:112–20.

[37] Horinouchi T, Morishima S, Tanaka T, Suzuki F, Tanaka Y, Koike K, et al. Pharmacological evaluation of plasma membrane β-adrenoceptors in rat hearts using the tissue segment binding method. Life Sc 2006;79:941–8.

[38] Lin CH, Yang CM, Chen CM, Ko FN, Teng CM. Pharmacological characteristics of BDTI, a new isoquinoline-derived β_2-adrenoceptor agonist, in canine trachea and rat heart. Pharmacology 1996;53:19–27.

[39] Klunder JM, Onami T, Sharpless KB. Arenesulfonate derivatives of homochiral building blocks for organic synthesis. J Org Chem 1989;54:1295–304.

[40] Van Dort ME, Jung YWJ, Sherman PS, Kilbourn MR, Wieland DM. Fluorine for hydroxysubstitution in biogenic amines: asymmetric synthesis and biological evaluation of fluorine-18-labelled β-fluorophenylalkylamines as model systems. J Med Chem 1995;38:810–5.

[41] Renner C, Höltke C, Wagner S, Faust A, Schober O, Kopka K, et al. Substitution der Hydroxylgruppe in einer Betablockerstruktur durch radioaktives Fluor. Nuklearmedizin 2009;48:A38.

[42] Louis SN, Rezmann-Vitti LA, Nero TL, Iakovidis D, Jackman GP, Louis WJ. CoMFA analysis of the human β_1-adrenoceptor binding affinity of a series of phenoxypropanolamines. Eur J Med Chem 2002;37:111–25.